Appl. Phys. B 69, 347–352 (1999) / Digital Object Identifier (DOI) 10.1007/s003409900181

Applied Physics B
Lasers
and Optics

Bragg spectroscopy and superradiant Rayleigh scattering in a Bose–Einstein condensate

J. Stenger, S. Inouye, D.M. Stamper-Kurn, A.P. Chikkatur, D.E. Pritchard, W. Ketterle

Department of Physics and Research Laboratory of Electronics, Massachusetts Institute of Technology, Cambridge, MA 02139, USA

Received: 26 June 1999/Revised version: 21 September 1999/Published online: 10 November 1999

Abstract. Two sets of studies concerning the interaction of off-resonant light with a sodium Bose–Einstein condensate are described. In the first set, properties of a Bose–Einstein condensate were studied using Bragg spectroscopy. The high momentum and energy resolution of this method allowed a spectroscopic measurement of the mean-field energy and of the intrinsic momentum distribution of the condensate. Depending on the momentum transfer, both the phonon regime as well as the free-particle regime could be explored. In the second set of studies, the cigar-shaped condensate was exposed to a single off-resonant laser beam and highly directional scattering of light and atoms was observed. This collective light scattering was caused by the long coherence time of the quasi-particles in the condensate and resulted in a new form of matter wave amplification.

PACS: 03.75.Fi; 32.80.Pj

What does a trapped Bose–Einstein condensate look like? More precisely, how does it interact with light, and does this differ fundamentally from what one would naively expect from a similar collection of very cold atoms? The experiments reviewed here all study off-resonant light scattering from a condensate, either spontaneously (i.e. Rayleigh scattering) or when stimulated by a second laser beam (i.e. Bragg spectroscopy). Light scattering imparts momentum to the condensate and creates an excitation which can be either a phonon or a free particle. A detailed study of the scattered light [1, 2], should therefore reveal a detailed picture of the Bose–Einstein condensate similar to the case of superfluid helium, where neutron scattering was used to obtain the spectrum of elementary excitations [3].

Since the light scattered from a typical 10^7-atom condensate is hard to detect, we used a second laser beam stimulating the scattering of light with a frequency and direction, which was pre-determined by the laser beam rather than post-determined by analyzing scattered light. This scheme, which we call Bragg Spectroscopy, establishes a high-resolution spectroscopic tool for Bose–Einstein condensates which is sensitive to the momentum distribution of the trapped condensate as well as the mean-field energy shift [4, 5]. We studied Bragg scattering in two regimes differing by the amount of momentum transfer. For large momentum excitations (free-particle regime) the resonance showed a Doppler broadening due to the zero-point motion of the condensate and a line shift and broadening due to the interactions within the condensate [4]. The observed Doppler broadening was consistent with the expected Heisenberg-uncertainty limited momentum distribution of a condensate with a coherence length equal to its physical size. For small momentum excitations (phonon regime) the light scattering rate was significantly reduced, providing evidence for the presence of correlated momentum excitations in the many-body condensate wavefunction [5].

More generally, Bragg spectroscopy can be used to determine the dynamic structure factor $S(\boldsymbol{q}, \nu)$ over a wide range of frequencies ν and momentum transfers $\boldsymbol{q}$ [6]. In contrast, the conventional imaging techniques like time-of-flight imaging or phase contrast imaging are not sensitive to the momentum distribution of a trapped condensate [7]. The spatial density distribution of the trapped condensate can be resolved in phase contrast imaging, and the momentum distribution of the atoms after being released from the trap can be imaged in time-of-flight. This momentum distribution, however, predominantly results from the released mean-field energy but not from the zero-point motion.

In a second set of studies we found that scattering of a single beam of light from the condensate led to a new process – self stimulated Rayleigh scattering – above a low threshold intensity [8]. We observed pulses of scattered light emanating from the ends of the condensate, establishing that this process is a new form of superradiance which occurs because the recoiling atoms remain coherent with the unscattered atoms, forming a matter wave grating which scatters subsequent photons in the same direction.

The two sets of studies shall be discussed in more detail in the following.

1 Bragg spectroscopy

Bragg spectroscopy was realized by exposing the condensate to two off-resonant laser beams with a frequency difference ν. The intersecting beams formed a moving interference pattern from which atoms could scatter when the Bragg condition was fulfilled (i.e. energy and momentum were conserved). The momentum transfer q and energy transfer $h\nu$ are given by $q = 2\hbar k \sin(\vartheta/2)$, where ϑ is the angle between the two laser beams with wave vector k. The process can also be driven in Nth order involving $2N$ photons, but only the first order shall be considered here. The Bragg scattering process can be thought of as the absorption of a photon from one laser beam and stimulated scattering into the second laser beam, and can be considered as the stimulated analog of neutron scattering which is used to study liquid helium.

The excitation spectrum for a weakly interacting homogeneous condensate at density n has the Bogoliubov form [9]

$$\nu = \sqrt{\nu_0^2 + 2\nu_0 nU/h}\,, \tag{1}$$

where $nU = n4\pi\hbar^2 a/m$ is the chemical potential, with a and m denoting the scattering length and the mass, respectively, and $h\nu_0 = q^2/2m$. For excitation energies much smaller than the chemical potential the excitation spectrum is phononlike, obeying $h\nu = cq$, where $c = \sqrt{nU/m}$ is the speed of sound [9]. For energies $h\nu \gg nU$ the spectrum is particlelike, obeying $h\nu = h\nu_0 + nU$.

The spectroscopic line shape $I(\nu)$ in the case of free-particle excitation in a homogeneous condensate would be a sharp peak. For a trapped condensate, however, the inhomogeneity of the density distribution broadens the peak. For our parabolic trapping potential the normalized density distribution reads $(15n/4n_0)\sqrt{1-n/n_0}$, where n_0 denotes the peak density. The simplest model for the spectroscopic lineshape $I_n(\nu)$ assumes that a volume element with local density n leads to a line shift nU/h:

$$I_n(\nu) \sim \frac{h(\nu-\nu_0)}{n_0 U}\sqrt{1-\frac{h(\nu-\nu_0)}{n_0 U}}\,, \tag{2}$$

which has an average value (first moment) of $4n_0U/7h$ and a rms-width of $\Delta\nu_n = \sqrt{8/147}n_0U/h$.

The observed line shape also depends strongly on the momentum distribution, since for a particle with momentum $\boldsymbol{p}$ the resonance frequency is Doppler-shifted by $\boldsymbol{qp}/mh$. The expected momentum distribution for a condensate trapped in a harmonic oscillator potential is given by the squared Fourier transform of the density distribution [10]. This results in a line shape which can be approximated by a Gaussian with an rms width

$$\Delta\nu_p = 1.699/2\pi m x_0\,. \tag{3}$$

This width is inversely proportional to the condensate size x_0 (Thomas-Fermi radius) and does not depend explicitly on the number of atoms.

In our experiments the broadening mechanisms represented by (2) and (3) have to be combined. While the exact calculation of the line shape requires detailed knowledge of the excitation wavefunctions, the total line shift (first moment) and rms-width can be calculated using sum rules and Fermi's Golden Rule. Thus, it can be rigorously shown that the total line shift remains $4n_0U/7h$, while the rms-width $\Delta\nu = \sqrt{\Delta\nu_n^2 + \Delta\nu_p^2}$ is the quadrature sum of the mean-field and the Doppler widths [11].

In our experiment a weak laser beam, with a frequency of 1.7 GHz red-detuned from the sodium $3S_{1/2}F = 1 \rightarrow 3P_{3/2}F = 0, 1, 2$ transition, was split into two beams in order to form the two Bragg beams [4, 12]. The beams were sent through two acousto-optical modulators driven at 80 MHz, but with a frequency difference corresponding to a recoil energy $q^2/2m$, of around 100 kHz when $q = 2\hbar k$. The laser beams were overlapped in a counterpropagating configuration, oriented in the radial direction of the cigar-shaped condensate, which was produced as in previous studies [13].

Figure 1 shows typical spectra, taken both for a trapped condensate and after 3 ms time of flight when the mean-field energy was fully converted into kinetic energy. Plotted is the relative number of Bragg-scattered atoms versus the frequency difference of the two Bragg beams (including an offset of $\nu_0 = 100$ kHz). The rms-width of the resonance for the ballistically expanding cloud is 20 kHz, which is much narrower than the 65-kHz-wide distribution of a thermal cloud at 1 μK, a typical value for the BEC transition temperature under our conditions. The spectra for the thermal cloud and the expanding condensate correspond to the spatial distributions observed by absorption imaging after sufficiently long time of flight. With this technique, the BEC transition is indicated by a sudden narrowing of the time-of-flight distribution by a factor of three. Using Bragg spectroscopy, the signature of BEC is much more dramatic – the condensate resonance is more than thirty times narrower than of the thermal cloud, and indeed narrower than that of the ground state of a single atom in the trap.

The resonance of the trapped condensate was studied as a function of the condensate density and size. Figure 2a demonstrates the linear dependence of the frequency shift on the density. The slope of the linear fit corresponds to $(0.54 \pm 0.07)\, n_0U/h$, in excellent agreement with the prediction of $4n_0U/7h$. Figure 2b shows the observed line width as function of the density. Figure 2c shows the line width as function of the condensate size after subtracting the mean-field broadening and an estimated experimental broadening (0.5 kHz) due to acoustic noise and the finite duration of the

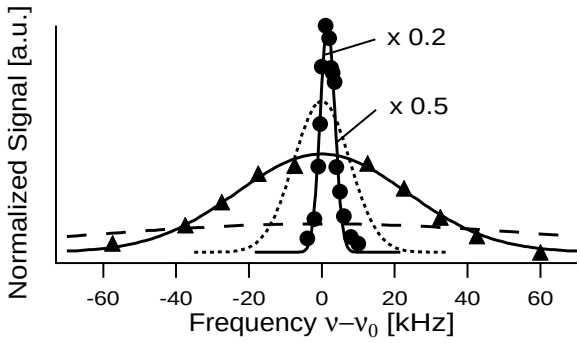

Fig. 1. Bragg resonances for a trapped condensate (*circles*) and after 3 ms time of flight (*triangles*). For comparison, the momentum distributions of the ground state of the trapping potential (*dots*) and of a 1-μK cold, thermal cloud (*dashes*) are indicated

Bragg pulse. The dashed line corresponds to a Heisenberg uncertainty limit in agreement with the expectations from (3), which demonstrates within our experimental uncertainties, that the coherence length of the condensate equals its physical size. In particular, our measurements indicate that the condensate does not have phase fluctuations, i.e. that it does not consist of smaller quasi-condensates with disjoint relative phases.

So far we have described Bragg spectroscopy of a Bose–Einstein condensate with a momentum transfer of two photon recoils, corresponding to a energy transfer $h\nu_0 = h100\,\mathrm{kHz}$ which is much larger than the chemical potential $n_0U/h < 10\,\mathrm{kHz}$. This is the particle regime (recoil velocity greater than speed of sound) where the line width mainly reflects the momentum distribution of individual atoms, modified by the mean-field energy.

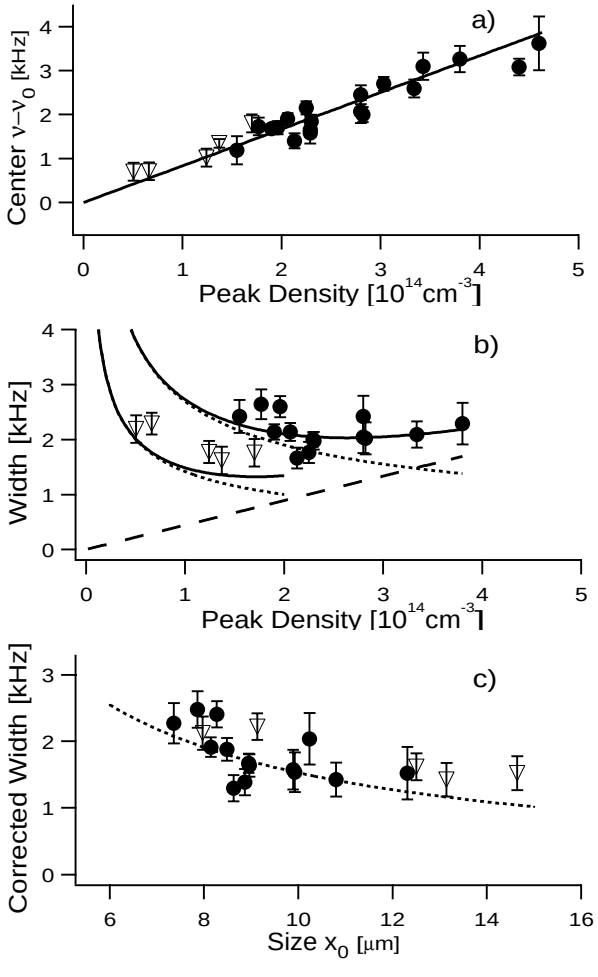

Fig. 2a–c. Bragg spectroscopy of a trapped condensate. Line shifts and widths are shown for various densities and sizes of the condensate using two different radial trapping frequencies, $\nu_r = (195 \pm 20)$ Hz (*circles*), and $\nu_r = (95 \pm 20)$ Hz (*triangles*). The lines in **b** show the contributions of the mean-field energy (*dashed*), due to the finite size (*dotted*, for both trapping frequencies), and their quadrature sum (*solid lines*). **c** displays the width after subtraction of the contributions of the mean-field and the finite pulse duration and compares it with the prediction for the momentum uncertainty due to the finite size. The error bars are 1σ errors of the Gaussian fits to the data

For small momentum transfer q with $q^2/2m \ll n_0U$, the condensate responds collectively and density perturbations propagate as phonons at the speed of Bogoliubov sound. The line shape at this small momentum transfer is dominated by the (inhomogeneous) mean-field energy and by phonon-like collective excitations. We have recently applied the Bragg beams at an angle of 14°, resulting in $q^2/2m = h \times 1.5\,\mathrm{kHz}$, well in the phonon regime [5]. The chosen momentum transfer corresponds to a reduced phonon wavelength (0.4 μm) much smaller than the condensate size (> 20 μm). This allows us to approximate the expected line shape using the Bogoliubov description of an interacting homogeneous Bose–Einstein condensate [14]. The parabolic density distribution of the trapped condensate can be included by a local density approximation leading to the line-center frequency being proportional to the square root of the density:

$$\nu_{\text{res-phonon}} = \frac{32}{15\pi}\sqrt{2\nu_0 n_0 U/h}\,, \tag{4}$$

compared to

$$\nu_{\text{res-free}} = \nu_0 + \frac{4}{7}\frac{n_0 U}{h} \tag{5}$$

in the free-particle regime.

This behavior was indeed observed when the chemical potential was varied from 0–10 kHz by changing the density of the condensate. Perhaps more importantly, the line strength was observed to be significantly smaller in the phonon regime than in the free-particle regime, providing striking evidence for the presence of correlated momentum excitations in the many-body condensate wavefunction. The normalized line strength is given by the static structure factor $S(\boldsymbol{q})$. In the phonon regime, it is reduced to $S(\boldsymbol{q}) \approx q/mc < 1$ compared to $S(\boldsymbol{q}) = 1$ in the free particle regime. These results are discussed in more detail in [5].

2 Rayleigh scattering

In the second set of studies we investigated the response of the condensate to a single, off-resonant laser beam [8]. The experimental setup was like the one used for Bragg spectroscopy, but with only one of the laser beams.

When the linear polarization of the light was chosen in the direction of the long axis of the condensate, just Rayleigh scattering was observed, as illustrated in Fig. 3b–d. A dramatic change occurred, when the polarization of the light was chosen perpendicular to this axis and when the intensity exceeded a threshold value of around $1\,\mathrm{mW/cm^2}$. As shown in Fig. 3e–f, the recoiled atoms were now ejected at an angle of 45° relative to both the long axis of the condensate and the direction of the incoming light. This effect can be understood as follows: When a condensate is exposed to a laser beam with wavevector $\boldsymbol{k}_0$ and scatters a photon with wavevector $\boldsymbol{k}_i$, an atom (or quasi-particle) with recoil momentum $\hbar\boldsymbol{K}_j = \hbar(\boldsymbol{k}_0 - \boldsymbol{k}_i)$ is generated. The presence of the recoiling atom constitutes a "memory" of the scattering and affects subsequent scattering events by interfering with the condensate at rest. This leads to a matter wave grating of wavevector $\boldsymbol{K}_j$, which diffracts the laser beam into the phase-matching direction $\boldsymbol{k}_i$ $(= \boldsymbol{k}_0 - \boldsymbol{K}_j)$. This diffraction

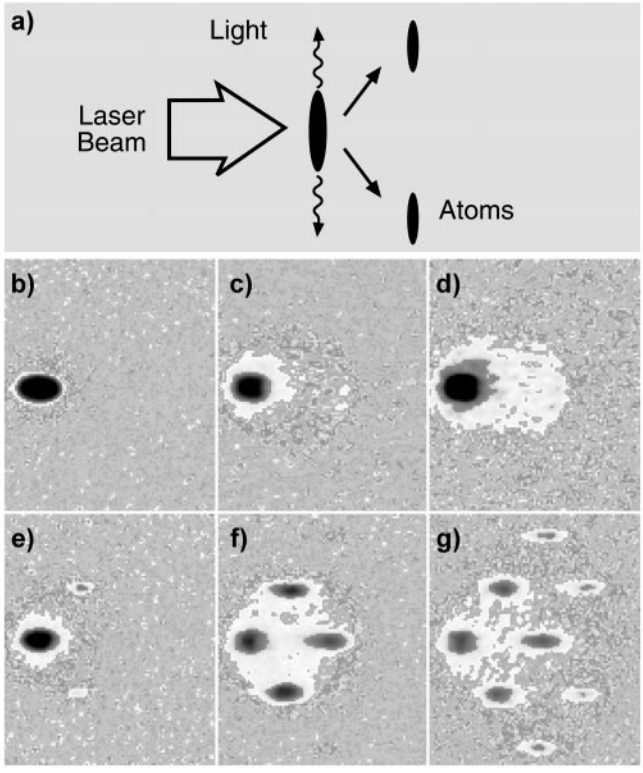

Fig. 3a–g. Observation of superradiant Rayleigh scattering. **a** A cigar-shaped condensate is illuminated with a single off-resonant laser beam. Collective scattering leads to photons scattered predominantly along the axial direction, and atoms at 45°. **b–g** Absorption images after 20 ms time-of-flight show the atomic momentum distribution after exposure of the atoms to a laser pulse of variable duration. When the polarization is parallel to the long axis, superradiance is suppressed, and normal Rayleigh scattering was observed (**b–d**). For perpendicular polarization, directional superradiant scattering of atoms was observed (**e–g**), and evolved to repeated scattering for longer laser pulses (**f**, **g**). The pulse durations are 25 μs (**b**), 100 μs (**c**, **d**), 35 μs (**e**), 75 μs (**f**), 100 μs (**g**). The field of view of each image is 2.8×3.3 mm. The scattering angle appears to be larger than 45° due to the angle of observation. All images use the same gray scale except for (**d**), which enhances the small signal of Rayleigh scattered atoms in **c**

is a self-amplifying process because every diffracted photon creates another recoiling atom which increases the amplitude of the matter wave grating. The observed emission of atoms at an angle of 45° originates from a recoil from the photon absorption process followed by a perpendicular emission of a photon along the condensate's long axis. An argument for this directionality of the emission is given below.

A more quantitative description for the matter wave amplification can be found quantum-mechanically. The basic Hamiltonian for Rayleigh scattering contains a sum of terms $g a^\dagger_i A^\dagger_j A_k a_l$ which can be regarded as four-wave mixing between two Schrödinger waves (A_j, A_k) and two electromagnetic waves (a_i, a_l). When, as is the case here, the light escapes so rapidly that the average number of photons in the system is much smaller than one, but the recoiling atoms remain in the volume of the condensate long after the scattering (the recoil velocity of sodium is 10 orders of magnitude slower than the speed of light), the transition rate is proportional to $(N_j + 1)$, where N_j is the number of atoms in the final state j. The growth rate of N_j can be obtained by using Fermi's Golden Rule and including a phenomenological loss term L_j:

$$\dot{N}_j = (R\, N_0\, \frac{\sin^2\theta_j}{8\pi/3}\, \Omega_j)\, (N_j + 1) - L_j N_j$$
$$= G_j (N_j + 1) - L_j N_j\ . \qquad (6)$$

Here, R denotes the rate for single-atom Rayleigh scattering, the angular term reflects the dipolar emission pattern with θ_j being the angle between the polarization of the incident light and the direction of emission, and Ω_j is the solid angle over which the phase-matching condition is fulfilled. The loss rate L_j predominantly arises from the decoherence of the recoiled atoms which leave the condensate after approximately $1/L_j \approx 35$ μs, limiting the memory time of the condensate for the matter wave grating.

It is the solid angle Ω_j which leads to the directionality of the amplified emission relative to the dipole pattern of spontaneous Rayleigh scattering. In our cigar-shaped condensate (aspect ratio about ten) the probability for emission of a subsequent photon into the same mode as a previous photon is highest along the long axis of the condensate, here $\Omega \sim \lambda^2/A$ is largest, since the geometrical projection of the condensate along this direction leads to the smallest cross-sectional area A (λ denotes the optical wavelength). This causes superradiance for photons emitted in this direction. The angular term in (6) containing θ_j explains the suppression of the superradiance when the polarization of the light is parallel to the long axis of the condensate.

The scattered light was directed onto a CCD camera in order to verify its directional emission (Fig. 4a). The camera was positioned out of focus of the imaging system, so that the images represent the angular distribution of photons emitted around the axial direction. The images consist of bright spots with an angular width equal to the diffraction limit for a source with a diameter $d \sim 14$ μm. Typical images showed several spots, and their pattern changed randomly even under the same experimental conditions. The observation of several spots is consistent with the geometric angle d/l, the ratio of the diameter d and the length l, being larger than the diffraction angle λ/d, which leads to multimode emission.

By replacing the camera with a photomultiplier, a time-resolved measurement of the scattered light intensity was obtained (Fig. 4b). Simple Rayleigh scattering would give a constant signal during the square-shaped laser pulse. Instead we observed a fast rise consistent with a stimulated process followed by a subsequent decay as the gain decreases in part due to the depletion of the condensate at rest.

The inset in Fig. 4b shows the time evolution of the second sequential process, corresponding to Fig. 3f or g, respectively. Subsequent emission occurs when the number of atoms having absorbed/scattered one pair of photons is large enough, so that the gain in this now moving part of the condensate overcomes the loss. Indeed, the observed onset of the second sequential process is delayed relative to the timing of the first scattering process, as shown in the inset in Fig. 4b. Subsequent four-wave mixing between matter waves [15] or stimulated Raman scattering may couple the different recoil modes and affect the observed distribution of atoms.

The observed effect of coherent directional emission of atoms, caused by superradiant Rayleigh scattering, can be

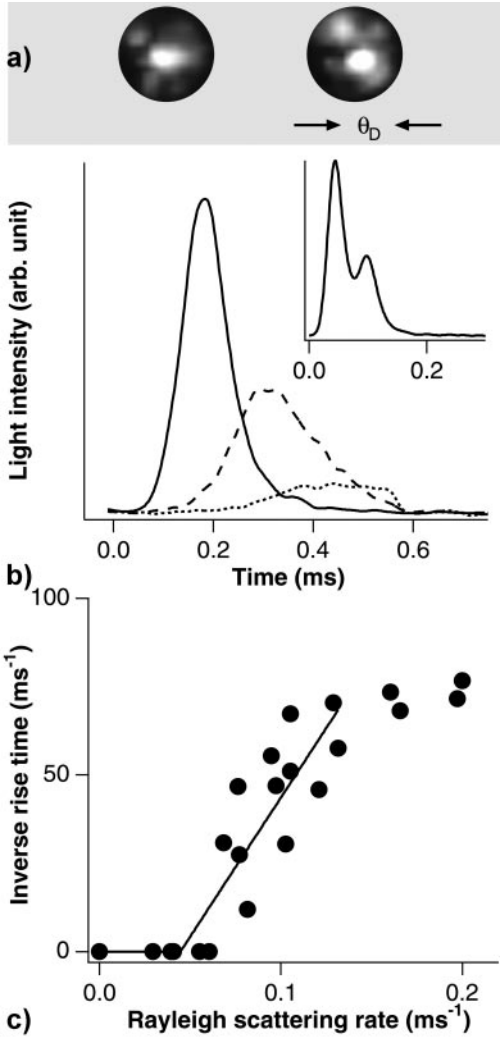

Fig. 4a–c. Observation of directional emission of light. **a** The angular pattern of the emitted light along the axial direction showed a few bright spots with an angular width corresponding to the diffraction-limited angle of an object of about 14 μm in diameter. The images were integrated over the entire duration of the light pulse. The *white circle* indicates the aperture of the imaging system. **b** The temporal evolution of the light intensity showed a strong initial increase characteristic of a stimulated process. For higher laser power, the pulse was shorter and more intense. The laser intensities were 3.8 mW/cm^2 (*solid line*), 2.4 mW/cm^2 (*dashed line*), and 1.4 mW/cm^2 (*dotted line*). The laser pulse duration was 550 μs. The *inset* shows a double peak in the temporal signal when the laser intensity was about 15 mW/cm^2, which was above the threshold for a second-order process. **c** The dependence of the inverse initial rise time vs. laser power shows a threshold for the stimulated process. The *solid curve* is a straight-line fit

compared to the case of the "coherence-brightened laser" as discussed by R.H. Dicke [16]. He describes an elongated radiating system of initially incoherently electronically excited atoms, and shows that this system realizes a laser in which the amplification is provided by electronic coherence even in the absence of mirrors to provide optical feedback. The key feature of this superradiance (or superfluorescence) [17] is that spontaneous emission is not a single-atom process, but a collective process of all atoms, leaving the atoms in a coherent superposition of ground and excited states which leads to a large dipole moment [16].

The phenomenon described in this paper is fully analogous: the condensate at rest "pumped" by the off-resonant laser corresponds to the electronically excited state in normal superradiance. It can decay by a spontaneous process to a state with photon recoil (corresponding to the ground state). The rate of superradiant emission in Dicke's treatment is proportional to the square of an oscillating macroscopic dipole moment. In the present case, the radiated intensity is proportional to the square of the contrast of the matter wave interference pattern between the condensate and the recoiling atoms. In both cases, the initial emission of light shows the single atom dipole pattern, but the greater solid angle of the "end-fire" modes in a highly elongated system gives them higher gain, leading to highly directional emission subsequently. One fundamental difference, however, is the occurance of sequential processes, which led to the "cascade" of recoiled atoms (Fig. 3f) and to the delayed emission of photons (inset in Fig. 4b).

3 Summary

The studies presented in this paper investigated the response of a Bose–Einstein condensate to one or two off-resonant laser beams. In both cases surprising effects could be observed due to the high temporal and spatial coherence of the condensate. The superior Doppler sensitivity of Bragg spectroscopy enabled the detection of sub-mm/s atomic velocities. Studied with this high resolution, the momentum distribution of the atoms was observed to depend inversely on the size of the condensate, demonstrating that its coherence length corresponds to its physical size. The strength of the Bragg spectroscopic signal (number of atoms receiving momentum) was found to be dramatically reduced in the phonon regime, showing that atoms in the Bose–Einstein condensate interact collectively, and weakly, with the light under these circumstances. When illuminated by a single laser beam, the long coherence time of the condensate led to a new form of superradiance – stimulated amplification of the number of recoiled atoms, with corresponding emission of Rayleigh scattered light in the direction of the long axis of the condensate. The low threshold for this effect should be considered in all experiments using optical probing and manipulation of Bose–Einstein condensates with off-resonant light.

Acknowledgements. This work was supported by the Office of Naval Research, NSF, Joint Services Electronics Program (ARO), NASA, and the David and Lucile Packard Foundation. A.P.C would like to acknowledge support from NSF, D.M.S.-K. from the JSEP Graduate Fellowship Program and J.S. from the Alexander von Humboldt-Foundation. J.S. is now at the Physikalisch Technische Bundesanstalt (PTB) Braunschweig, Germany.

References

1. J. Javanainen: Phys. Rev. Lett. **75**, 1927 (1995); R. Graham, D. Walls: Phys. Rev. Lett. **76**, 1774 (1996); A.S. Parkins, D.F. Walls: Phys. Rep. **303**, 1 (1998), and references therein
2. H.D. Politzer: Phys. Rev. A **55**, 1140 (1997)
3. P. Sokol: In *Bose–Einstein condensation*, ed. by A. Griffin, D.W. Snoke, S. Stringari (Cambridge University Press 1995); P. Nozières, D. Pines: *The Theory of Quantum Liquids* (Addison-Wesley, Reading 1994)
4. J. Stenger et al.: Phys. Rev. Lett. **82**, 4569 (1999)

5. D. Stamper-Kurn et al.: Phys. Rev. Lett. **83**, 2876 (1999)
6. see e.g.: T.J. Greytak: In *Quantum Liquids*, ed. by J. Ruvalds, T. Regge: (North-Holland 1978); P. Nozieres, D. Pines: *The theory of quantum liquids* (Addison-Wesley, Redwood City, CA 1990)
7. W. Ketterle, D.S. Durfee, D.M. Stamper-Kurn: In *Bose–Einstein condensation in atomic gases, Proceedings of the Intern. School of Physics 'Enrico Fermi'*, ed. by M. Inguscio, S. Stringari, C.E. Wieman: /IOS Press, Amsterdam 1999); E.A. Cornell, J.R. Ensher, C.E. Wieman: ditto
8. S. Inouye et al.: Science **285**, 571 (1999)
9. K. Huang: *Statistical Mechanics*, 2nd edn. (Wiley, New York 1987)
10. G. Baym, C.J. Pethick: Phys. Rev. Lett. **76**, 6 (1996)
11. D. Stamper-Kurn: PhD thesis, MIT 1999
12. M. Kozuma et al.: Phys. Rev. Lett. **82**, 871 (1999)
13. M.-O. Mewes et al.: Phys. Rev. Lett. **77**, 416 (1996)
14. N.N. Bogoliubov: J. Phys. (USSR) **11**, 23 (1947)
15. L. Deng et al.: Nature **398**, 218 (1999)
16. R.H. Dicke: Phys. Rev. **93**, 99 (1954); R.H. Dicke: In *Proceedings of the third international congress on Quantum Electronics*, ed. by P. Grivet, N. Bloembergen (Columbia University press, New York 1964) pp. 35–54
17. N. Skribanowitz, I.P. Herman, J.C. MacGillivray, M.S. Feld: Phys. Rev. Lett. **30** 309 (1973); R. Bonifacio, L.A. Lugiato: Phys. Rev. A **11** 1507 (1975); M.F.H. Shuurmanns, Q.H.F. Vrehen, D. Polder, H.M. Gibbs: In *Advances in Atomic and Molecular Physics* (1981) pp. 167–228; Q.H.F. Vrehen, H.M. Gibbs: In *Topics in Current Physics 27*, ed. by R. Bonifacio (Springer, Berlin, Heidelberg 1982) pp. 111–147; M. Gross, S. Haroche: Phys. Rep. **93**, 301 (1982)